Anal Bioanal Chem (2015) 407:4035–4044
DOI 10.1007/s00216-015-8620-7

RESEARCH PAPER

Comparison of sp-ICP-MS and MDG-ICP-MS for the determination of particle number concentration

Sabrina Gschwind · Maria de Lourdes Aja Montes · Detlef Günther

Received: 27 August 2014 / Revised: 28 February 2015 / Accepted: 4 March 2015 / Published online: 22 March 2015

Abstract In 2011, the European Commission introduced new regulations on how nanomaterials are defined. Since then, researchers have emphasized that more complete characterization of nanoparticles (NPs) includes not just mass and size determinations, but also the determination of the particle number concentrations. In this study, two different sample introduction approaches for the analysis of NP suspensions with inductively coupled plasma mass spectrometry (ICP-MS) were investigated: pneumatic nebulization (sp-ICP-MS) and microdroplet generation (MDG-ICP-MS). These approaches were compared for the determination of particle number concentrations (PNCs) of gold and silver NP suspensions diluted in either ultra-pure water or citrate solution. For accurate sp-ICP-MS analysis, it is crucial to know the transport efficiency of nebulized sample into the plasma. Here, transport efficiencies, measured by the waste collection method, were 11–14 % for Ag suspensions and 9–11 % for Au. In contrast, the droplet transport efficiency of MDG-ICP-MS was 100 %. Analysis by sp-ICP-MS yielded a lower particle number concentration than expected (only 20–40 % of the expected value), whereas MDG-ICP-MS had NP recoveries up to 80 %. This study indicates that NP reference materials are of major importance for particle number determination and detailed results on particle number concentrations for different suspensions with respect to storage time are discussed.

Keywords Microdroplet generation · ICP-MS · Nanoparticle · Particle number concentration · sp-ICP-MS

Introduction

Nanomaterials are used in many fields due to their unique properties [1–5], even though little is known about their impact on the environment or human health. Therefore, it is important to characterize these materials carefully. The most critical properties to assess are mass, size, morphology, elemental composition, and particle number concentration (PNC).

In 2011, the European Commission proposed new directions about the definition of nanoparticles (NP) [6]. According to these new regulations, a nanomaterial is a natural, incidental, or manufactured material that contains particles in an unbound state, as aggregate or agglomerate, and where 50 % or more of the particles have at least one dimension in the nanoscale range (<100 nm).

Inductively coupled plasma mass spectrometry (ICP-MS) allows for the fast and sensitive determination of most elements, and has recently been used for the analysis of NPs for mass, composition, and PNC [7].

Apart from ICP-MS analysis, PNC determination in liquid samples can be carried out using various other techniques, such as dynamic light scattering (DLS) [8], laser-induced breakdown detection (LIBD) [9], transmission/scanning electron microscopy (TEM/SEM) [10], or NP tracking analysis (NTA) [11]. However, DLS is fundamentally limited to the measurement of mass concentrations of approximately 10–

Electronic supplementary material The online version of this article (doi:10.1007/s00216-015-8620-7) contains supplementary material, which is available to authorized users.

S. Gschwind · D. Günther (✉)
Department of Chemistry and Applied Biosciences, Laboratory of Inorganic Chemistry, ETH Zurich, Vladimir-Prelog Weg 1, 8093 Zürich, Switzerland
e-mail: guenther@inorg.chem.ethz.ch

M. d. L. Aja Montes
Institute of Chemistry and Biochemistry, ZHAW Wädenswil, Einsiedlerstrasse 41, 8820 Wädenswil, Switzerland

100 mg kg^{-1} [8]. LIBD and NTA are also insensitive to the concentrations below 10^6 particles mL^{-1} [9, 11]. Finally, counting particles by electron microscopy is very time consuming and requires a homogeneous, single-layer deposition of the NPs on a sample grid [10].

In 2003, Degueldre et al. first reported the introduction of highly dilute particle suspensions into the ICP by conventional nebulization in order to obtain the mass distribution and concentration of particles simultaneously [12]. Following, this concept has been applied for various particle types [13–16]. In 2009, Allabashi et al. [17] and Hu et al. [18] rediscovered the potential of ICP-MS for single particle analysis, and since then, the number of laboratories promoting ICP-MS for NP analysis has grown [19–23]. However, this method bears some significant challenges. Specifically, the pneumatic nebulizers typically used for sp-ICP-MS produce polydisperse aerosol that passes through a spray chamber, in which most of the liquid is lost due to collision with the chamber's wall (loss up to 99 %). Therefore, with this setup, the quantification of the introduced NPs is only possible if the aerosol transport efficiency (TE) is known, where TE is defined as the ratio of the volume reaching the plasma to the initially nebulized volume. Several methods to measure the aerosol TE have been proposed by Pace et al. [24]. Two of these methods use an Au NP reference material (NIST) and are based on the application of either known NP size or known PNC for further calculations. On the other hand, a third method, called the *waste collection method*, determines the TE based on the measurement of sample uptake rate and waste, and is the only method which does not rely on NP reference material. Nevertheless, this method yielded an overestimated TE and, in turn, an approximately 50 % lower mass concentration when compared to the other strategies [24]. Currently, no data on how much the measured PNC deviates from the expected PNC after dilution of the original suspension have been reported. Clearly, TE determination for sp-ICP-MS is challenging, and a method that introduces well-defined amounts of liquid with 100 % transport efficiency into the ICP-MS might overcome the shortcomings of particle introduction by pneumatic nebulization. Specifically, it would eliminate the laborious determination of the TE, and its associated error, while still knowing the introduced liquid volume per time interval.

The microdroplet generator (MDG) delivers discrete low-volume samples, and has been used for the introduction of single particles into an ICP-optical emission spectrometer (OES) [25–27] or ICP-MS [28–31], the introduction of single cells into an ICP-MS [32], and for fundamental studies on plasma-droplet interactions and effects [33–38]. Due to the very low sample uptake, the matrix does not affect the analysis and even liquids containing high salt contents or organic solutions can be used.

It has been shown that MDG-ICP-MS can be used for the quantification of the mass/size of metallic and metal oxide NPs either by internal or external calibration without using any particle-based reference material [29] and can be used for simultaneously accessing ionic and particulate fraction of various elements using a time-of-flight (ToF) ICP-MS [30].

MDG-ICP-MS and sp-ICP-MS can both be used to quickly measure PNCs. However, if the concentration is too high, i.e., if statistically more than one NP per dwell time enters the plasma and is measured, the samples must be diluted, which can influence the sample and the stability of the NPs in the suspension. If the dilution is not appropriate, the NPs will be analyzed in bulk mode (several NPs together, results averaged) and no information about individual NPs can be gained [19]. However, NPs are normally not very abundant in environmental samples and dilution can be neglected (predicted environmental concentration (PEC)$<10^6$ particles mL^{-1}, ng kg^{-1} to μg kg^{-1}) [39–41]. On the other hand, low PNCs will require longer acquisition times, but not necessarily additional treatment, e.g., enrichment which might alter the appearance of the NPs. When using the MDG, the sample introduction volume can be easily increased by changing the nozzle sizes from 30 μm (droplet size ~40 μm) to 70 μm (droplet size ~90 μm) or by increasing the introduction frequency without changing the droplet TE of 100 %.

In this study, suspensions of silver (Ag) and gold (Au) NPs of various concentrations were used for the quantification of PNC. The original suspensions were diluted to three different concentrations and measured after different storage times (up to 1 week) to track the sample alteration across time with either sp-ICP-MS or MDG-ICP-MS. Because of the different uptake rates and acquisition parameters, the suspensions had to be diluted more when analyzed by sp-ICP-MS than for MDG-ICP-MS.

For sp-ICP-MS, the TE was determined for each sample during each measurement by the waste collection method. The MDG was optimized for 100 % TE and for an introduction with regular temporal spacing between the droplets. The results obtained for the two different techniques were compared and limitations and further conclusions for absolute particle number quantification are given.

Materials and methods

Samples

Three suspensions containing different Ag NP sizes (60, 80, and 100 nm [0.02 mg mL^{-1} in 2 mM citrate, NanoComposix, San Diego, USA]), and a certified reference gold nanoparticle suspension (60 nm, 0.05 mg mL^{-1}, RM 8013, NIST®, Gaithersburg, MD, USA), were used in this study. The certified values are provided in Table 1.

Table 1 Certified values reported by the suppliers, uncertainties for the original PNC was calculated including uncertainty from size measurement

	60 nm Ag	80 nm Ag	100 nm Ag	60 nm Au
Size (TEM) (nm)	57.4±4.0	78.9±3.9	99.4±7.0	56.0±0.5
Mass concentration (μg kg^{-1})	0.021	0.023	0.021	0.052
Original PNC (mL^{-1})	$2.0\pm0.4\times10^{10}$	$8.5\pm1.3\times10^{9}$	$3.9\pm0.8\times10^{9}$	$2.9\pm0.1\times10^{10}$

The total metal content of each Ag suspension was quantified prior to the measurements according to the method presented in Hagendorfer et al. [42] using indium (In) as recovery standard and diluting the samples to approximately 1 μg kg^{-1} with 1 % (*v*/*v*) HNO_3 (sub boiled). Au NP digestion was performed using concentrated aqua regia with rhodium (Rh) as the recovery standard and dilution after digestion with 1 % (*v*/*v*) HCl (Trace Select, Sigma-Aldrich, Buchs, Switzerland) to approximately 1 μg kg^{-1}. Iridium (Ir) was used for Ag and Au quantification as internal standard.

To identify the amount of dissolved Au and Ag in the original suspension, 200 μL of the suspension was diluted to 5 mL with purified water (18 MΩ cm, Millipore, Billerica, MA, USA) and centrifuged for 1 h at 7000×*g*. The sample vial was carefully opened and 2 mL of the supernatant was extracted. It was important to prevent NP re-dispersion by moving the vial. The supernatant was divided and then diluted with either ultra-pure water to check if NPs were still present or 1 % (*v*/*v*) HNO_3/HCl and the respective IS for quantification of Au and Ag concentrations.

The certified sizes of the NPs were verified using SEM.

For PNC measurements, each sample was diluted to three different initial concentrations with purified water or 2 mM citrate (sodium citrate tribasic dehydrate BioUltra, Sigma-Aldrich, Buchs, Switzerland) following the procedure described earlier [29]. Each dilution was measured subsequently after different storage times (directly after preparation (time 0), 5, 24, 48, 72, and 175 h later) by MDG-ICP-MS and sp-ICP-MS. Between measurements, the solutions were stored in the dark at 5 °C. For the MDG measurements, the suspensions were diluted to a final particle number concentration of approximately 10^6–10^7 particles mL^{-1}, and to ~10^3–10^5 particles mL^{-1} for sp-ICP-MS to minimize the probability of having more than one NP measured per dwell time. Theoretical PNCs calculated from the dilution factors can be found in Table 2.

MDG-ICP-MS

A microdroplet generator (MDG, Microdrop Technologies GmbH, Norderstedt, Germany) with a nozzle diameter of 30 μm was connected horizontally to a sector field (SF) ICP-MS instrument (Element 2, ThermoFisher, Bremen, Germany) as described elsewhere [29]. Operating conditions are summarized in Table 3. The mean diameter of the droplets was ~34 μm and the generation frequency was 100 Hz resulting in a typical volume aspirated of 120 nL min^{-1}.

The generated droplets were constantly monitored for stability and size using a CCD camera. Before each measurement, a video was recorded and the droplet size and subsequent volume was determined with a custom-written macro for the open source graphic program ImageJ [43].

Each sample was measured for 15 or 30 min for MDG and for 55 min for sp-ICP-MS to achieve suitable statistics, i.e., until 1×10^3–2×10^4 NPs were measured.

sp-ICP-MS

A pumped, low-flow enhanced parallel-path nebulizer (Arimist, Burgener Research Inc, Canada) with an uptake of approximately 250 μL min^{-1} was coupled to a Scott double-pass spray chamber (PFA Pure Chamber, Elemental Scientific, Germany) and to the ICP-SF-MS. The transport efficiency was determined using the waste collection method described by Pace et al. [24] and Gustavsson [44]. For this purpose, an empty vial and the sample-containing vial were weighed. Prior to starting the nebulizer pump, the waste tubing was connected to the waste vial. The pump was then started and measurements were conducted for 55 min; after analysis, the

Table 2 Expected particle number concentrations after dilution for the different suspensions with either ultra-pure water (H_2O) or 2 mM citrate (citrate) for MDG-ICP-MS (MDG) or sp-ICP-MS measurements

	Au NIST 60 nm	Ag 60 nm	Ag 80 nm	Ag 100 nm
MDG H_2O PNC1 (mL^{-1})	2.7×10^6	1.5×10^6	6.2×10^5	2.9×10^5
MDG H_2O PNC2 (mL^{-1})	1.4×10^7	7.3×10^6	3.1×10^6	1.4×10^6
MDG H_2O PNC3 (mL^{-1})	2.9×10^7	3.9×10^7	6.2×10^6	2.9×10^6
MDG Citrate PNC1 (mL^{-1})		1.7×10^6	1.5×10^6	1.2×10^6
MDG Citrate PNC2 (mL^{-1})		8.1×10^6	7.4×10^6	6.1×10^6
MDG Citrate PNC3 (mL^{-1})		1.7×10^7	1.5×10^7	1.3×10^7
sp-ICP-MS H_2O PNC1 (mL^{-1})	8.4×10^3	4.9×10^4	4.8×10^4	4.5×10^4
sp-ICP-MS H_2O PNC2 (mL^{-1})	1.7×10^4	1.4×10^5	1.0×10^5	1.4×10^5
sp-ICP-MS H_2O PNC3 (mL^{-1})	2.5×10^4	4.6×10^5	5.1×10^5	4.8×10^5

Table 3 Operating conditions for MDG-ICP-MS and sp-ICP-MS

	MDG-ICP-MS	sp-ICP-MS
Plasma gas flow (L min^{-1})	16	16
Auxillary gas flow (L min^{-1})	~1–1.2	~0.85
Sample gas flow (L min^{-1})	~1.2	~1.0
Helium gas flow (L min^{-1})	~0.4	None
Plasma power (W)	1280	1280
Dwell time (ms)	1	10
Samples/peak	1000	1000
Integration window	10 %	10 %
Runs	2000	200
Mass resolving power	~300	~300
No. of measurements	5 or 10	3

pump was stopped and both vials were removed and weighed. The TE was calculated using the following formula.

$$\mathrm{TE} = \frac{\Delta m_{\mathrm{up}} - \Delta m_{\mathrm{waste}}}{\Delta m_{\mathrm{up}}} \quad (1)$$

where Δm_{up} and $\Delta m_{\mathrm{waste}}$ represent the differences in mass [g] for the sample and the collected waste found during the measurement, respectively.

Data evaluation

The recorded data was processed in MATLAB (2012b, MathWorks, Natick, USA) to eliminate the background signals, apply a so called "split correction," which is necessary for MDG-ICP-MS measurements when integration times less than 10 ms are used (for details, see elsewhere [29]), and to convert the intensity, in counts per second, to raw counts. The reduced data set was transferred to Origin 8.6 (OriginLab Corporations, Northampton, USA) for subsequent analysis. In Origin, the signals were binned and plotted as an intensity distribution, and fitted with a multiple Gauss functions to resolve signals corresponding to one, two, three, or more NPs (see Electronic Supplementary Material (ESM) for an example of Au).

To calculate the total number of measured particles, the number of events under the first Gauss distribution peak (corresponding to one NP per droplet) was summed. The number of events under the second and multiple Gauss distribution peaks were multiplied by the appropriate NP number and summed. The total number of measured NPs is given as the sum of NP events under all intensity distribution peaks.

To determine PNC, the counted particles in a given time window were divided by the introduced liquid volume within the same period of time. For MDG, the total volume was calculated by multiplying the volume of an individual droplet by the number of introduced droplets (number of produced droplets during measurement). For the nebulizer, the liquid volume was obtained by multiplying the uptake rate by the TE and the measurement duration. The original PNC was then calculated by dividing the obtained PNC by the dilution factor used during sample preparation.

In addition to the individual results obtained for each of the three concentrations of each sample, the mean PNC value for each measurement was calculated. The "real" PNCs reported here, are the averages of the PNC determinations from the three different concentrations of each sample; the standard deviation (SD) was also determined.

Results

Calculation of PNC from total metal content and NP size determination

The NPs used here are synthesized by bottom-up approach, and especially the Ag NPs are known to undergo dissolution with time. Therefore, it was important to quantify the total metal content, as well as the total dissolved metal in the suspension for PNC calculation of the original suspension. This was conducted by either digestion or Ag/Au quantification of the original suspension, or ultracentrifugation of the suspension and subsequent analysis of the supernatant. To ensure that all particles were centrifuged, part of the supernatant was diluted 1:5 with H_2O (minimizing probability of dissolution due to acidic environment) and measured by sp-ICP-MS. No particle signals above the elevated background intensity originating from dissolved material were observed.

Ag and Au concentrations in the supernatant (from ionic or dissolved content) after centrifugation were subtracted from the total Au and Ag content of the NP suspensions in order to determine the metal concentration from the particulate fraction. Furthermore, the SEM measurements enabled to verify the certified NP size.

From this information, the particle number concentration was calculated, assuming that the NPs have a density similar to pure Au or Ag metal, respectively, using the following formula (2):

$$\mathrm{PNC} = \frac{c_{\mathrm{particulate}}}{4/3 \times \pi \times {r_{\mathrm{NP}}}^3 \times \rho} \quad (2)$$

Where $c_{\mathrm{particulate}}$ is the mass concentration of the particulate fraction, r_{NP} is the radius of the NP, and ρ is the density. The results are summarized in Table 4. The total mass concentration for Ag differs by approximately 10 % from the value given by the manufacturer. Considering the loss due to ionic Ag (5 %), only 85 % of the reported value by the supplier can be used for the PNC calculation. Au differs by 2 %.

Table 4 Certified sizes and measured metal concentration; subsequent calculation of the particulate fraction and PNC determined for four different particle types

NP suspension	Size (nm)	Total metal concentration (mg/mL)	Particulate (mg/mL)	PNC (mL^{-1})
Ag 60 nm	57.4±4.0	0.0188±0.0003	0.0182±0.0003	$1.8±0.4×10^{10}$
Ag 80 nm	78.9±3.9	0.0210±0.0003	0.0202±0.0003	$7.5±1.2×10^{9}$
Ag 100 nm	99.4±7.0	0.0187±0.0010	0.0181±0.0010	$3.4±0.9×10^{9}$
Au 60 nm	56.0±0.5	0.0514±0.0011	0.0514±0.0011	$2.9±0.1×10^{10}$

Additionally, error propagation was included into the calculation of the PNC. From that, it is visible that the RSD increases up to, e.g., 26 % (Ag 100 nm), which is dominated by the uncertainty of the size measurements, which is also apparent in the calculated PNC from the manufacturer's data in Table 1.

Particle number concentration of Au NP suspension

Figure 1a shows the linear dependence of the number of particles measured by MDG-ICP-MS directly to dilution compared to the expected PNCs. The error bars correspond to the standard deviation of 10 replicates (t=3 min 23 s, each). The slope of the measured PNCs differs from the expected PNCs. The measured values were approximately 23–39 % lower when compared to the expected PNC. The R^2 of the linear regression was 0.998. For sp-ICP-MS, the deviation from the expected value was between 54 and 64 % (see Fig. 1b). The error bars show the standard deviation of three measurements (T=16 min 40 s, each). Even though the number of particles was corrected for the different TEs obtained for each measurement, the linearity of the fit represented by R^2 was only 0.965. The TEs for the three different concentrations at time 0 were 9.3, 8.8, and 9.4 %, respectively, which are in the same range as reported by Pace et al. [24] using a similar introduction system. When using the particle frequency-based calculation for the TE proposed by Pace et al. [24], the TE only results in 3.5 %.

The PNCs that were determined after various storage times for sp-ICP-MS and MDG-ICP-MS are shown in Fig. 2a. Figure 2b provides the mean PNCs of the three dilutions at each storage time. For both graphs, the PNCs in the original sample were calculated, with dilution accounted for, to allow a valuable comparison between the three different solutions measured at both different times and with either sp-ICP-MS and MDG-ICP-MS. As it can be seen from all measurements, the PNC at all storage times was lower than the expected number concentration.

For MDG-ICP-MS, the most diluted NP suspension (PNC1) shows the lowest recovery (61 % directly after preparation), whereas the other two NP suspensions provided results closer to the expected PNC (77 and 83 %). Concentrations 2 and 3 generally trend to lower PNCs over time, most likely due to NP losses, e.g., sticking to the vial wall. However, this PNC loss is most pronounced at the beginning (until 3 h), and afterwards stabilizes (recovery ~58 and 66 %, respectively). For concentration 1, the PNC seems to increase over time. This might be explained by particles sticking to the capillary of the MDG in the beginning of experiments, which is then slowly washed out of the capillary until equilibrium is reached. The recovery for PNC1 increases from 61 to 86 %. Ionic Au was for all measurements below the limits of detection. This can be explained by the fact that Au NPs are stable and less prone to oxidation and further dissolving processes.

For sp-ICP-MS, the recoveries were significantly lower. At time 0, only 46 % (PNC1) to 38 % (PNC3) of the expected

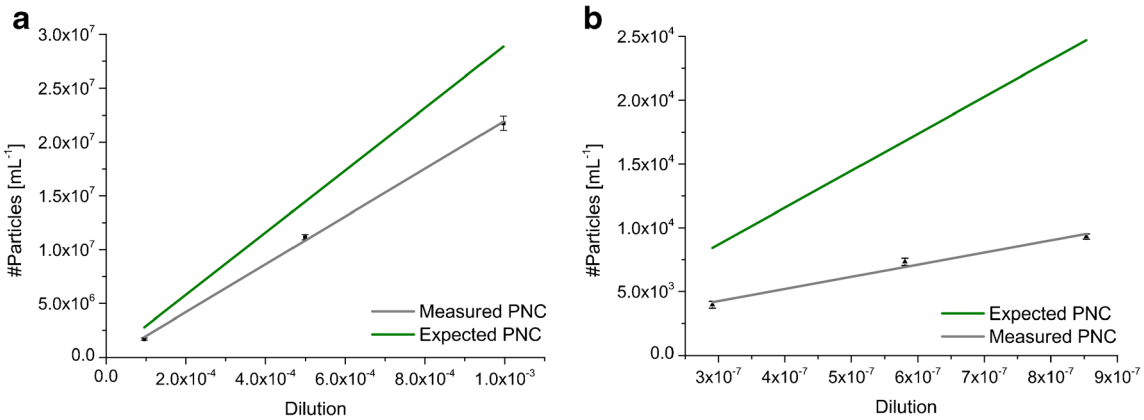

Fig. 1 Linear dependence of the number of detected particles per introduced volume of the measurements at time 0 as a function of the dilution (*gray*) (MDG: $y=-2.6×10^5+2.2×10^{10}x$, R^2=0.998; sp: $y=1400+9.6×10^9x$, R^2=0.965). The *green line* shows the expected concentrations of the original PNC diluted for MDG-ICP-MS (**a**) and diluted for sp-ICP-MS (**b**) measurements

particle number was detected. For the lowest concentration, the recovery first decreases (43 and 39 %) and remains stable until the last measurement after 47 h (43 %). The concentration in dilution 2 decreased over time (38, 40, and 31 %) whereas dilution 3 showed an initial increase followed by a decrease (38, 44, and 40 %). However, the results for sp-ICP-MS obtained for the different dilution factors at the different times were more reproducible than those obtained with MDG-ICP-MS; the relative standard deviations vary only between 6 % (23 h) and 17 % (47 h) (Fig. 2b).

Particle number concentration of Ag NP suspension

The original NP suspension was stabilized in 2 mM citrate. To compare the effect of the stabilizer at high dilution, the suspension was diluted either with ultra-pure water or with 2 mM citrate solution.

The linear dependence of the measured NPs at time 0 versus the dilution factor are displayed in Fig. 3a for the MDG-ICP-MS setup and in Fig. 3b for sp-ICP-MS. Again, the slope was higher for the samples measured by MDG-ICP-MS compared to sp-ICP-MS; however, there is a significant difference between the samples diluted in citrate and those diluted in H_2O. The values determined for the citrate-based suspensions were close to the expected PNC; however, the linearity was worse than for H_2O.

If instead of the TE obtained by the waste collection method, the calculated TE by the particle frequency method from the Au NIST reference material is used (TE=3.5 %), the calculated PNCs for Ag are almost the same as the expected one. Only for the highest concentrated suspension (PNC3), the calculated value is still 50 % off.

The determined PNCs at several storage times for the individual suspensions of 60 nm Ag NPs are shown in Fig. 4a. To assess whether there is a drift in PNCs over longer storage times, the suspensions were measured by sp-ICP-MS again after the storage time of 1 week.

All determined recoveries were below 100 %. However, the results were inconsistent and show large variations for the different concentrations of NP suspensions. For example, the PNC determined with MDG-ICP-MS for the dilutions made using citrate stabilization differ least from the expected concentrations; however, the lowest concentration (PNC1) provided a 95 % NP recovery, and the intermediate and highest concentrations (PNC2 and PNC3) were 52 and 68 %, respectively. Over time, the value for PNC2 and PNC3 show a trend towards lower values, for PNC1 the recovery for the measurements after 3 h was below 20 %, but increased with time again to more than 60 %.

The PNCs determined by MDG-ICP-MS in water also show a rather "random" behavior after dilution. For example, the recoveries for the lowest concentration varied from 30 to 3 % to 15 % to final value as low as 2 %. The PNC for the medium concentration decreased from 50 to 10 % after 48 h and the highest concentration decreased from 50 to 15 % with a minimum after 24 h to as low as 6 % recovery. The measurements conducted with the pneumatic nebulizer provided more reproducible results with decreasing values over time. However, the recoveries at time 0 were only 38, 30, and 21 % for the lowest, middle, and highest concentrations, respectively.

When comparing the mean PNCs for each experimental set over time (Fig. 4b), the water-diluted sample sets measured by either sp- or MDG-ICP-MS resulted in similar PNCs and decreased over time. However, the SD was smaller for the sp-ICP-MS measurements. The RSD was approx. 20 % for the first four measurements and increased to 80 % for the longest storage time. The citrate-stabilized NP solutions showed the highest recovery decreasing slightly over time.

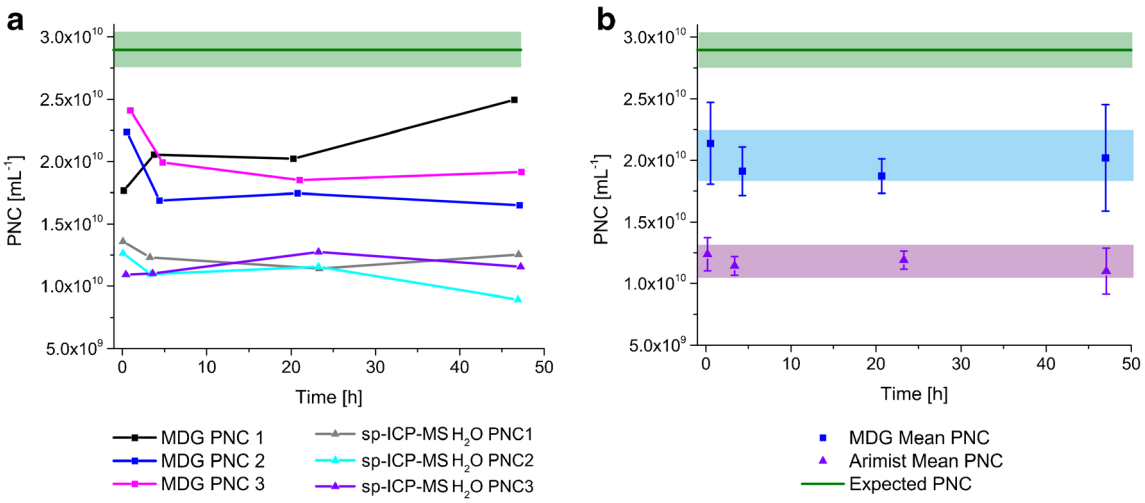

Fig. 2 **a** Expected PNC (*green*) including the error and the determined particle number concentrations for 60 nm Au NP suspensions for three different concentrations (*black*, *blue*, *violet*) in two different experiments (*square* and *triangle*). The original suspension was diluted with H_2O to the concentration required for single particle events in the ICP. **b** Mean values for PNC1, PNC2, and PNC3 for the different experiments: suspension diluted with H_2O and measured with MDG (*blue square*), suspension diluted with H_2O and measured with sp-ICP-MS (*violet triangle*)

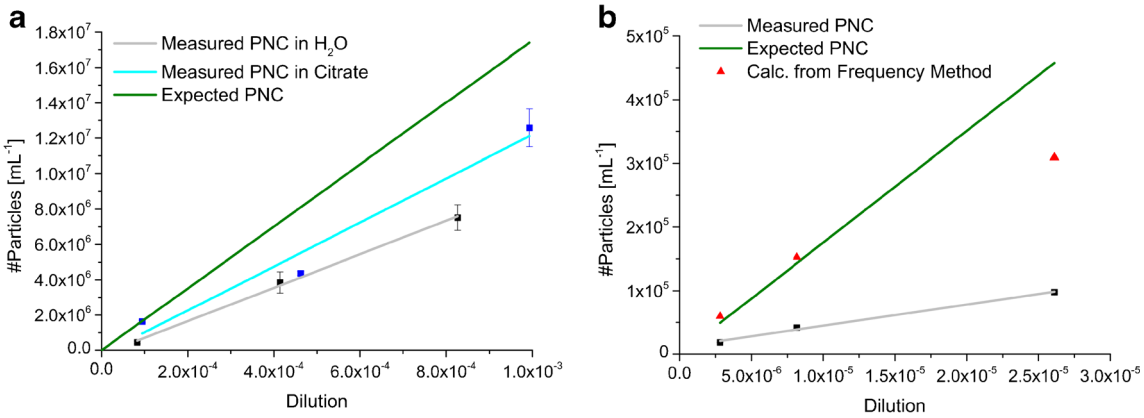

Fig. 3 Linear dependency of the number of detected particles (Ag 60 nm) per introduced volume of the measurements at time 0 as a function of the dilution in water (*gray*, MDG: $y=-2\times10^5+9.5\times10^9x$, $R^2=0.996$ and sp: $y=1\times10^4+3.3\times10^9x$, $R^2=0.991$) or citrate (*blue*, $y=-2\times10^5+1.2\times10^{10}x$, $R^2=0.939$). The *green line* shows the expected concentrations of the original PNC diluted for MDG-ICP-MS (**a**) and diluted for sp-ICP-MS (**b**) measurements. The *red triangles* (**b**) represent the calculated PNC using a TE of 3.5 % obtained by the particle frequency method for the NIST Au NPs

The results for the silver NPs of 80 and 100 nm are summarized in the ESM. They were not very reproducible and are rather difficult to explain. The analyses performed by MDG-ICP-MS show the largest deviations between the different dilution factors, as well as between the different storage times. However, the mean values for MDG-ICP-MS were closer to the expected concentration than sp-ICP-MS.

Discussion and conclusion

When calculating the PNC from mass concentration, it is important to keep in mind that the shape of the NPs can differ from a perfect sphere [29] (see TEM micrographs provided from the manufacturer for Ag and an SEM micrograph for Au in the ESM, Fig. S1 to S4), which can cause significant discrepancies in PNC calculations. The analysis of bulk silver by ICP-MS revealed that the purchased Ag samples contained 10 % less silver than quoted. Only about 85 % of the reported silver was present in particulate form and 5 % of the reported silver was in ionic form. The certified gold concentration differed by less than 2 % and no ionic Au was detected. Limits of detection for Au and Ag NPs were 13 and 11 nm, respectively, which represents almost the current limits of ICP-MS and were therefore not limiting parameters in this study.

Transport efficiencies determined for the nebulizer/spray chamber system used in this study, were between 9 and 11 % for Au and 11 to 14 % for Ag, respectively. Because the two experiments were not conducted at the same time, it is most likely, that this deviation was caused by day to day

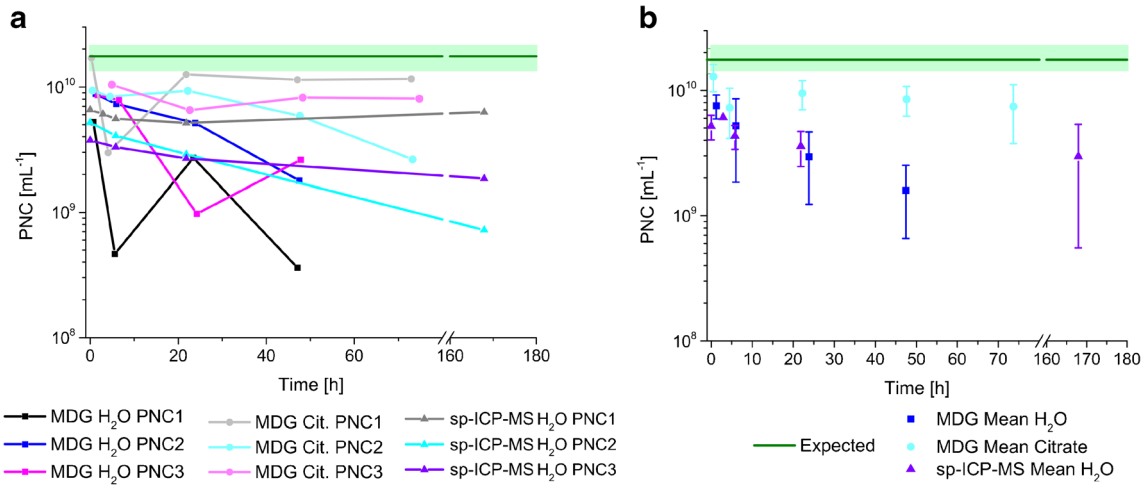

Fig. 4 **a** Expected PNC (*green*) and determined particle number concentration for a 60 nm Ag NP suspension for three different concentrations (*black*, *blue*, *violet*) in three different experiments (*square*, *circle*, and *triangle*). The *square* and *triangle symbols* belong to the suspension diluted with H_2O, and the *circle symbol* to the suspension diluted with 2 mM citrate. **b** Mean values for PNC1, PNC2, and PNC3 for the different experiments: suspension diluted with H_2O and measured with MDG, *blue square*; suspension diluted with 2 mM citrate and measured with MDG, *cyan sphere;* and suspension diluted with H_2O and measured with sp-ICP-MS, *violet triangle*

variation in the optimization procedure of the ICP-MS. This study shows no indication that the aerosol TE is dependent on the size, composition, or concentration of the NPs. However, Au and Ag were studied within similar size ranges and concentrations (concentration range differed only by one order of magnitude). Therefore, it is not unlikely that, for more diverse suspensions of NP and other NP materials, NP-specific TEs can occur.

The measured PNCs deviate more than 20 % from the expected PNC for both Ag and Au nanoparticles. Even though the Au NPs do not dissolve, and were taken from a certified reference material, it was not possible to determine a recovery of 100 %. However, the recovery for Au was approximately 20 % higher than for Ag. Unfortunately, the PNCs calculated do not follow a systematic trend. For different experiment series, more or fewer particles were detected. As expected, citrate stabilized the 60 nm Ag particles better than H_2O and higher recoveries were found. However, the citrate-based suspensions for the 80 and 100 nm NPs show lower recoveries (see ESM).

When comparing the reproducibility for the different suspensions measured by sp-ICP-MS or MDG-ICP-MS, Au shows similar results for both types of introduction systems (RSD between 6 and 20 %), whereas, for the Ag suspensions, the MDG setup provided more significant deviations. The differences between the results for different concentrations measured were much higher for Ag NPs (RSD >30 % vs. <20 %).

In general, the poor and erratic recoveries might be explained by one or a combination of reasons:

1. NPs might stick to different parts of the sample introduction system
2. NPs might be missed during the settling time of the detector; this effect is probably minor on the instrument used for this study
3. Probability of losing droplets that contain NPs might be different due to surface charge, which can cause attraction or repulsion,
4. Inaccurate measurements of the transport efficiency
5. Over- or underestimation of the expected PNC due to a different density than the pure metal, which was assumed for the PNC calculations (PNC inversely proportional to the density).

Depending on the surface charge of the NPs, sticking to the walls of the capillary and the vial is likely and can result in an uncontrolled release of the particles. Even though a 100 % transport efficiency of the droplets can be achieved with the microdroplet dispenser (reported in [28, 29]), it is not guaranteed that 100 % of the NPs will be transported to the ICP. The stability of the NP suspension and the sampling position in the vial can also influence the TE of NPs. By increasing the measurement time, the influence of NP sticking, and the subsequent release of NPs, might be reduced and average out. However, a longer measurement time is not favorable due to more expensive analysis and drifts, which might occur in the ICP-MS.

Pace et al. [24] showed that better results can be achieved with sp-ICP-MS using a reference material for calculating the mass concentration and size of an unknown NP suspension when compared to the waste collection method, which is limited by the availability of reference materials. Currently, it remains unknown how much different NP types and concentrations are influenced when they are sprayed and travel through a spray chamber (including secondary release of such materials). When the recoveries obtained for the Au NPs (used as reference material by Pace et al. [24]) and the Ag NPs are compared, they show similar results (40 % versus 20–30 %) for a similar aspiration rate and TE. When using the frequency method proposed by Pace et al. [24], assuming a known PNC concentration of the NIST particles and calculating the TE, the TE results in 3.5 %, which is much lower than the TE obtained by the waste collection method. Applying this value for calculating the PNC of the Ag suspensions, the resulting PNCs were only deviating by ±10 % from the expected concentrations for most of the analyzed suspensions (see Fig. 3b).

As is expected, Ag NPs dissolve slowly. This is confirmed by an increase of the intensity of the ionic fraction of Ag over time (data not shown). The dissolution of the Ag NPs should be minimized in the samples containing more citrate because citrate is used not only for stabilization against agglomeration of the NPs, but also as reducing agent to reduce Ag^+ to Ag^0 (reported as the Turkevich method) [45, 46]. However, no significant changes between water and citrate diluted samples were determined.

Compared to the PNC obtained by using sp-ICP-MS, MDG-ICP-MS showed a higher overall recovery. Additionally, MDG-ICP-MS has a lower uptake rate (120 nL min^{-1} vs. 250 μL min^{-1}), a much higher TE (100 % vs. 10 %), and a shorter dwell time (1 ms vs. 10 ms) when compared to sp-ICP-MS.

The MDG-ICP-MS benefits from less dilution of the samples, less interaction with different materials (no nebulizer or spray chamber), production of monodisperse droplets, and 100 % transportation of these droplets into the plasma. However, the results are less reproducible.

For further studies on PNC, it will be important to ensure that the sample preparation does not affect the properties of the NPs such as shape, agglomeration, or degradation. In addition, for sp-ICP-MS, it is necessary to keep in mind that, for the method proposed by Pace et al. [24], a NP reference material (Au NIST RM) must be used for the quantification of Ag NPs. It is still not clear how much the transportation behavior of different kinds of NPs is influenced by using different introduction systems,

different concentrations, sizes, or compositions compared to the reference material; this requires further study.

The MDG approach currently suffers from poor reproducibility and long measurement times in order to obtain representative sampling of natural samples. Therefore, both the sp-ICP-MS and MDG-ICP-MS methods need significant improvements before sampling and quantification of nanomaterials can be routinely carried out on real samples.

Acknowledgments The authors would like to thank Dr. Frank Krummeich at the EMEZ (Electron Microscopy ETH Zurich) for SEM measurements. Financial support by ETH Zurich, Switzerland (ETH-4912-2) is gratefully acknowledged.

References

1. Alivisatos AP (2001) Less is more in medicine—sophisticated forms of nanotechnology will find some of their first real-world applications in biomedical research, disease diagnosis and, possibly, therapy. Sci Am 285(3):66–73
2. Wise K, Brasuel M (2011) The current state of engineered nanomaterials in consumer goods and waste streams: the need to develop nanoproperty-quantifiable sensors for monitoring engineered nanomaterials. Nanotechnol Sci Appl 4(1):73–86
3. Nischwitz V, Goenaga-Infante H (2012) Improved sample preparation and quality control for the characterisation of titanium dioxide nanoparticles in sunscreens using flow field flow fractionation on-line with inductively coupled plasma mass spectrometry. J Anal At Spectrom 27:1084–1092
4. Schneider OD, Weber F, Brunner TJ, Loher S, Ehrbar M, Schmidlin PR, Stark WJ (2009) In vivo and in vitro evaluation of flexible, cottonwool-like nanocomposites as bone substitute material for complex defects. Acta Biomater 5(5):1775–1784
5. Gowda SR, Leela Mohana Reddy A, Zhan X, Ajayan PM (2011) Building energy storage device on a single nanowire. Nano Lett 11(8):3329–3333
6. Commission E (2011) Commission Recommendation of 18 October 2011 on the Definition of Nanomaterial. vol 2011/696/EU. Off. J. Eur. Comm
7. Laborda F, Bolea E, Jiménez-Lamana J (2013) Single particle inductively coupled plasma mass spectrometry: a powerful tool for nanoanalysis. Anal Chem 86(5):2270–2278
8. HORIBA L (2014) Particle Characterization SZ-100. http://www.horiba.com/scientific/products/particle-characterization/education/sz-100/particle-size-by-dynamic-light-scattering-resources/choosing-concentration-for-dls-size-measurement/. Accessed 5 Dec 2014
9. Bitea C, Walther C, Kim JI, Geckeis H, Rabung T, Scherbaum FJ, Cacuci DG (2003) Time-resolved observation of ZrO2-colloid agglomeration. Colloids Surf A 215(1–3):55–66
10. Dudkiewicz A, Tiede K, Loeschner K, Jensen LHS, Jensen E, Wierzbicki R, Boxall ABA, Molhave K (2011) Characterization of nanomaterials in food by electron microscopy. TrAC Trends Anal Chem 30(1):28–43
11. Gallego-Urrea JA, Tuoriniemi J, Hassellöv M (2011) Applications of particle-tracking analysis to the determination of size distributions and concentrations of nanoparticles in environmental, biological and food samples. TrAC Trends Anal Chem 30(3):473–483
12. Degueldre C, Favarger PY (2003) Colloid analysis by single particle inductively coupled plasma-mass spectroscopy: a feasibility study. Colloids Surf A 217(1–3):137–142
13. Degueldre C, Favarger PY (2004) Thorium colloid analysis by single particle inductively coupled plasma-mass spectrometry. Talanta 62(5):1051–1054
14. Degueldre C, Favarger PY, Bitea C (2004) Zirconia colloid analysis by single particle inductively coupled plasma-mass spectrometry. Anal Chim Acta 518(1–2):137–142
15. Degueldre C, Favarger PY, Rosse R, Wold S (2006) Uranium colloid analysis by single particle inductively coupled plasma-mass spectrometry. Talanta 68(3):623–628
16. Degueldre C, Favarger PY, Wold S (2006) Gold colloid analysis by inductively coupled plasma-mass spectrometry in a single particle mode. Anal Chim Acta 555(2):263–268
17. Allabashi R, Stach W, de la Escosura-Muñiz A, Liste-Calleja L, Merkoçi A (2009) ICP-MS: a powerful technique for quantitative determination of gold nanoparticles without previous dissolving. J Nanopart Res 11(8):2003–2011
18. Hu S, Liu R, Zhang S, Huang Z, Xing Z, Zhang X (2009) A new strategy for highly sensitive immunoassay based on single-particle mode detection by inductively coupled plasma mass spectrometry. J Am Soc Mass Spectrom 20(6):1096–1103
19. Krystek P, Ulrich A, Garcia CC, Manohar S, Ritsema R (2011) Application of plasma spectrometry for the analysis of engineered nanoparticles in suspensions and products. J Anal At Spectrom 26: 1701–1721
20. Laborda F, Jimenez-Lamana J, Bolea E, Castillo JR (2011) Selective identification, characterization and determination of dissolved silver(I) and silver nanoparticles based on single particle detection by inductively coupled plasma mass spectrometry. J Anal At Spectrom 26(7):1362–1371
21. Mitrano DM, Barber A, Bednar A, Westerhoff P, Higgins C, Ranville J (2012) Silver nanoparticle characterization using single particle ICP-MS (SP-ICP-MS) and asymmetrical flow field flow fractionation ICP-MS (AF4-ICP-MS). J Anal At Spectrom 27:1131–1142
22. Reed R, Higgins C, Westerhoff P, Tadjiki S, Ranville J (2012) Overcoming challenges in analysis of polydisperse metal-containing nanoparticles by single particle inductively coupled plasma mass spectrometry. J Anal At Spectrom 27:1093–1100
23. Tuoriniemi J, Cornelis G, Hassellöv M (2012) Size discrimination and detection capabilities of single-particle ICPMS for environmental analysis of silver nanoparticles. Anal Chem 84(9):3965–3972
24. Pace HE, Rogers NJ, Jarolimek C, Coleman VA, Higgins CP, Ranville JF (2011) Determining transport efficiency for the purpose of counting and sizing nanoparticles via single particle inductively coupled plasma mass spectrometry. Anal Chem 83(24):9361–9369
25. Garcia CC, Murtazin A, Groh S, Becker M, Niemax K (2010) Characterization of particles made by desolvation of monodisperse microdroplets of analyte solutions and particle suspensions for nanoparticle calibration in inductively coupled plasma spectrometry. Spectrochim Acta, Part B 65(1):80–85
26. Garcia CC, Murtazin A, Groh S, Horvatic V, Niemax K (2010) Characterization of single Au and SiO_2 nano- and microparticles by ICP-OES using monodisperse droplets of standard solutions for calibration. J Anal At Spectrom 25:645–653
27. Murtazin A, Groh S, Niemax K (2010) Measurement of element mass distributions in particle ensembles applying ICP-OES. J Anal At Spectrom 25(9):1395–1401
28. Gschwind S, Flamigni L, Koch J, Borovinskaya O, Groh S, Niemax K, Günther D (2011) Capabilities of inductively coupled plasma mass spectrometry for the detection of nanoparticles carried by monodisperse microdroplets. J Anal At Spectrom 26(6):1166–1174
29. Gschwind S, Hagendorfer H, Frick DA, Günther D (2013) Mass quantification of nanoparticles by single droplet calibration using inductively coupled plasma mass spectrometry. Anal Chem 85(12): 5875–5883
30. Borovinskaya O, Hattendorf B, Tanner M, Gschwind S, Günther D (2013) A prototype of a new inductively coupled plasma time-of-

flight mass spectrometer providing temporally resolved, multi-element detection of short signals generated by single particles and droplets. J Anal At Spectrom 28(2):226–233
31. Franze B, Strenge I, Engelhard C (2012) Single particle inductively coupled plasma mass spectrometry: evaluation of three different pneumatic and piezo-based sample introduction systems for the characterization of silver nanoparticles. J. Anal. At. Spectrom. (27):1074-1083
32. Shigeta K, Traub H, Panne U, Okino A, Rottmann L, Jakubowski N (2013) Application of a micro-droplet generator for an ICP-sector field mass spectrometer—optimization and analytical characterization. J Anal At Spectrom 28:646–656
33. Chan GCY, Zhu Z, Hieftje GM (2012) Effect of single aerosol droplets on plasma impedance in the inductively coupled plasma. Spectrochim Acta, Part B 76:87–95
34. Chan GCY, Zhu Z, Hieftje GM (2012) Operating parameters and observation modes for individual droplet analysis by inductively coupled plasma-atomic emission spectrometry. Spectrochim Acta, Part B 76:77–86
35. Flamigni L, Koch J, Wiltsche H, Brogioli R, Gschwind S, Günther D (2012) Visualization, velocimetry, and mass spectrometric analysis of engineered and laser-produced particles passing through inductively coupled plasma sources. J Anal At Spectrom 27(4):619–625
36. Olesik JW, Gray PJ (2012) Considerations for measurement of individual nanoparticles or microparticles by ICP-MS: determination of the number of particles and the analyte mass in each particle. J Anal At Spectrom 27:1143–1155
37. Borovinskaya O, Aghaei M, Flamigni L, Hattendorf B, Tanner M, Bogaerts A, Günther D (2014) Diffusion- and velocity-driven spatial separation of analytes from single droplets entering an ICP off-axis. J Anal At Spectrom 29(2):262–271
38. Koch J, Flamigni L, Gschwind S, Allner S, Longerich H, Günther D (2013) Accelerated evaporation of microdroplets at ambient conditions for the on-line analysis of nanoparticles by inductively-coupled plasma mass spectrometry. J Anal At Spectrom 28(11):1707–1717
39. Gottschalk F, Sonderer T, Scholz RW, Nowack B (2009) Modeled Environmental concentrations of engineered nanomaterials (TiO_2, ZnO, Ag, CNT, fullerenes) for different regions. Environ Sci Technol 43(24):9216–9222
40. Fabrega J, Luoma SN, Tyler CR, Galloway TS, Lead JR (2011) Silver nanoparticles: behaviour and effects in the aquatic environment. Environ Int 37(2):517–531
41. Boxall A, Chaudhry Q, Sinclair C, Jones A, Aitken R, Jefferson B, Watts C (2007) Current and future predicted environmental exposure to engineered nanoparticles. Central Science Laboratory, York, UK
42. Hagendorfer H, Kaegi R, Parlinska M, Sinnet B, Ludwig C, Ulrich A (2012) Characterization of silver nanoparticle products using asymmetric flow field flow fractionation with a multidetector approach—a comparison to transmission electron microscopy and batch dynamic light scattering. Anal Chem 84(6):2678–2685
43. Rasband WS, *U.S. National of Health, Bethesda, MA, USA*, 1997–2012, http://imagej.nih.gov/ij/
44. Gustavsson A (1984) The determination of some nebulizer characteristics. Spectrochim Acta, Part B 39(5):743–746
45. Turkevich J, Stevenson PC, Hillier J (1951) A study of the nucleation and growth processes in the synthesis of colloidal gold. Discuss Faraday Soc 11:55–75
46. Lee PC, Meisel D (1982) Adsorption and surface-enhanced Raman of dyes on silver and gold sols. J Phys Chem 86(17):3391–3395